Supporting Information:

Role of Cyano-Substitution in Distyrylbenzene Derivatives on the Fluorescence and Electroluminescence Properties

Chuan Li[a], Muddasir Hanif[a], Xianglong Li[a], Shitong Zhang[b], Zengqi Xie[a,*], Linlin Liu[a,*], Bing Yang[b], Shijian Su[a], Yuguang Ma[a,*]

[a]*Institute of Polymer Optoelectronic Materials and Devices, State Key Laboratory of Luminescent Materials and Devices, South China University of Technology, Guangzhou 510640, P. R. China.*
Tel: +86-20-22237035; Fax: +86-20-87110606
E-mail: msxiez@scut.edu.cn; msliull@scut.edu.cn; ygma@scut.edu.cn

[b]*State Key Laboratory of Supramolecular Structure and Materials, Jilin University, Changchun 130012, P. R. China.*

Table of Contents

1. Experimental Section

General Information

All the reagents and solvents used for the synthesis and characterization were purchased from Aldrich and Acros and used without further purification. The ^{1}H and ^{13}C NMR data were recorded on a Bruker ASCEND 500 spectrometer at 500 MHz, using tetramethylsilane (TMS) as the internal standard, CDCl$_3$ and DMSO-d_6 as solvent. The MALDI-TOF-MS mass spectra were measured using an AXIMA-CFRTM plus instrument. Thermal gravimetric analysis (TGA) was measured on a Perkin-Elmer thermal analysis system from 30 ℃ to 900 ℃ at a heating rate of 10 K/min under nitrogen flow rate of 80 mL/min. Differential scanning calorimetry (DSC) was performed on a NETZSCH (DSC-204) unit from 30 ℃ to 400 ℃ at a heating rate of 10 K/min under nitrogen atmosphere. The electrochemical properties were carried out via cyclic voltammetry (CV) measurements by using a standard one-compartment, three-electrode electrochemical cell given by a BAS 100B/W electrochemical analyzer. Tetrabutylammoniumhexafluorophosphate (TBAPF$_6$) in anhydrous acetonitrile (CH$_3$CN) (0.1 M) were used as the electrolyte for negative or positive scan. A glass-carbon disk electrode was used as the working electrode, a Pt wire as the counter electrode, Ag/Ag$^+$ as the reference electrode together with ferrocene as the internal standard at the scan rate of 100 mV/s. Ag/Ag$^+$ reference electrode is commercially available and is constituted of (1) a silver wire; (2) AgNO$_3$ solution (0.01 M) in which the AgNO$_3$ is solute and acetonitrile is solvent and (3) tetrabutylammoniumhexafluorophosphate (TBAPF$_6$) (0.1 M) which is used as supporting electrolyte. UV-vis and fluorescence spectra were recorded on a Shimadzu UV-3100 spectrophotometer using 1 cm path length quartz cells. The fluorescence lifetime and PLQY (Φ_F) of solid film were measured by FLS920 Spectrometer. The Φ_F of different solutions was determined by using 0.1 M quinine sulfate as a reference ($\Phi_F = 0.546$) and were calculated by using the following formula:

$$Q_x = Q_r \left(\frac{A_r(\lambda_r)}{A_x(\lambda_x)}\right)\left(\frac{I(\lambda_r)}{I(\lambda_x)}\right)\left(\frac{n_x^2}{n_r^2}\right)\left(\frac{D_x}{D_y}\right)$$

where Q is the PLQY, A is the value of absorbance, I is the intensity of excitation source, n is the refractive index of solvent, D is the area of emission spectra, λ is the corresponding

wavelength. The subscript r stands for the reference while x stands for test subject. The excitation wavelength was 347 nm.

Device Fabrication

ITO coated glass was used as the substrate and the sheet resistance was 20 U square^{-1}. The ITO glass substrates were cleaned with isopropyl alcohol, acetone, toluene and deionized water, dried in an oven at 120 °C, treated with UV-zone for 20 min, and finally transferred to a vacuum deposition system with a base pressure lower than 5×10^{-6} mbar for organic and metal deposition The deposition rate of all organic layers was 1.0 A s^{-1}. The cathode LiF (1 nm) was deposited at a rate of 0.1 A s^{-1} and then the capping Al metal layer (100 nm) was deposited at a rate of 4.0 A s^{-1}. The electroluminescent (EL) characteristics were measured using a Keithley 2400 programmable electrometer and a PR-650 Spectroscan spectrometer under ambient condition at room temperature.
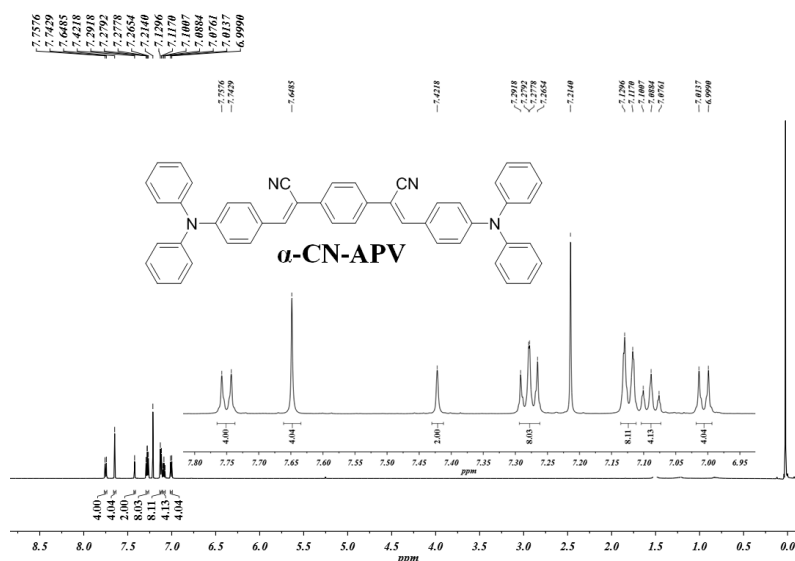
The radiative exciton yield can be calculated from the following equation: EQE = $\gamma \times \Phi_{PL} \times \eta_r \times \eta_{out}$ where EQE is the maximum external quantum efficiency, γ is the carrier recombination efficiency, which in the ideal case is supposed to be unity if the injected holes and electrons are fully recombined and degrade to excitons in the emissive layer, Φ_{PL} is the PLQY of the emission layer, η_r is the radiative exciton yield, and η_{out} is light out-coupling efficiency, which is 20% if there are not any out-coupling enhancing structures in the device.

Computational Details

The ground-state (S_0) and the lowest singlet excited state (S_1) geometries were optimized at the B3LYP/6-31G(d, p) level, which is a common method to provide molecular geometries and the optimized outcome is in good agreement with the experiment result. The HOMO/LUMO distributions are calculated on the basis of optimized S_0 state.

2. Synthesis and Characterization

Synthesis of α-CN-APV: Under an argon atmosphere, the triphenylamine formaldehyde (4 mmol) and terephthaloyl acetonitrile (2 mmol) were dissolved in the mixed solvents tert-butanol (6 mL) and tetrahydrofuran (8 mL). The mixture of solution was slowly heated up to 50 ^{o}C, and then potassium *t*-butoxide (0.02 mmol) and TBAH (0.02 mmol, 1M in methanol) were rapidly injected. After 90 minutes, the reaction mixture was poured into methyl alcohol, acidified with acetic acid. Suspension was subjected to suction filtration, and then washed with methanol washed twice to obtain a tan colored solid 670 mg, yield 50.3%. ^{1}H NMR (600 MHz, CDCl$_3$, ppm): δ 7.75-7.74 (d, 4H), 7.64 (s, 4H), 7.42 (s, 2H), 7.29-7.26 (t, 8H), 7.12-7.11 (d, 8H), 7.10-7.07 (t, 4H), 7.01-6.99 (d, 4H). ^{13}C NMR (CDCl$_3$, 125 MHz, ppm): δ 149.1, 145.4, 140.8, 134.1, 129.8, 128.5, 125.08, 124.7, 123.5, 119.6, 117.5, 105. FTIR (KBr, wavenumber, cm^{-1}): 3060, 3028, 2203, 1650, 1582, 1484, 1415, 1328, 1270, 1192, 1177, 1070, 1025, 994, 897, 824, 754, 693, 616, 531. MALDI-TOF (mass m/z): 666.34 [M$^+$]; calcd for C$_{48}$H$_{34}$N$_4$: 666.28.

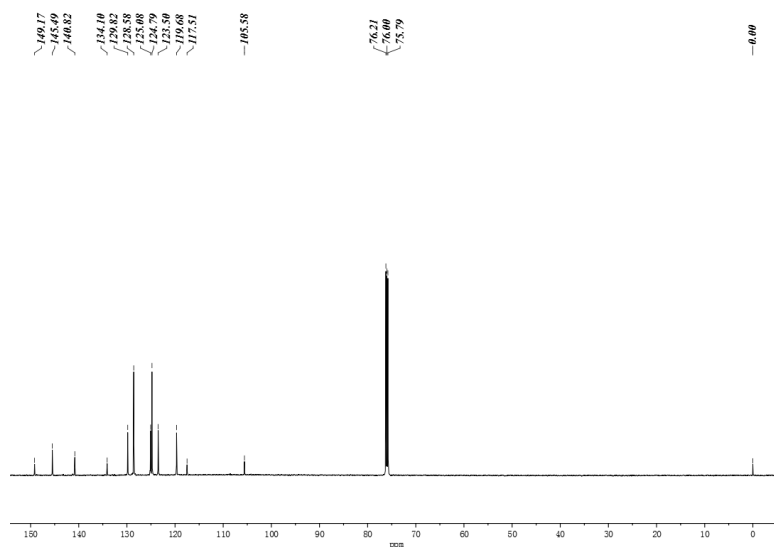**Figure S1**. ^{1}H NMR (600 MHz, CDCl$_3$) of α-CN-APV (inset shows the expanded aromatic region)

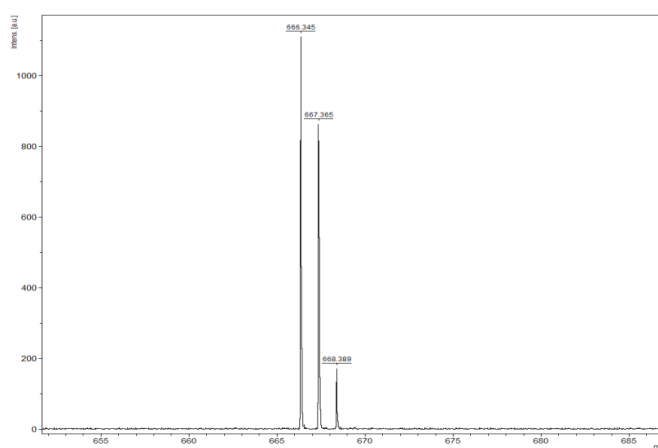**Figure S2**. ^{13}C NMR (150 MHz, CDCl$_3$) of α-CN-APV

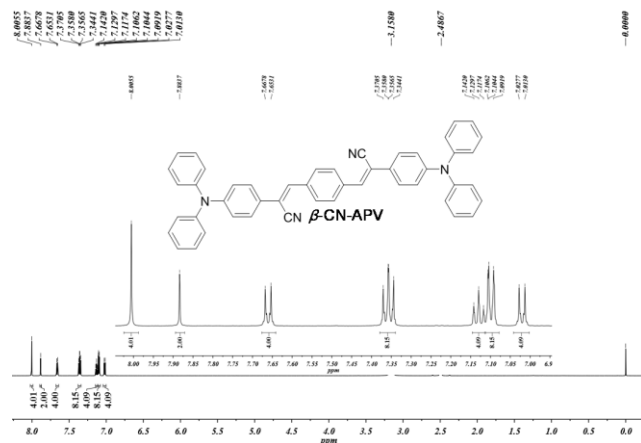**Figure S3**. Mass Spectrum (MALDI-TOF) of α-CN-APV.

Synthesis of β-CN-APV:

Under an argon atmosphere, the triphenylamine acetonitrile (3 mmol) and terephthalaldehyde (1.5 mmol) were dissolved in tert-butanol (6 mL) and Tetrahydrofuran (8 mL), and heated to 50 $^{\circ}$C. Potassium *t*-butoxide (0.015 mmol) and TBAH (0.015 mmol, 1M solution in methanol) was rapidly injected. After 90 minutes, the reaction mixture was acidified with acetic acid and poured into methyl Alcohol. After filtration, the solid was washed with methanol several times, to give a red solid 539 mg yield 54.0%. ^{1}H NMR (500 MHz, DMSO-d_6, ppm): δ 8.00 (s, 4H), 7.88 (s, 2H), 7.66-7.65 (d, 4H), 7.37-7.34 (t, 8H), 7.14-7.11 (t, 4H), 7.10-7.09 (d, 8H), 7.02-7.01 (d, 4H).^{13}C NMR (CDCl$_3$, 125 MHz, ppm): δ 148.1, 145.9, 137.0, 134.4, 128.4, 126.1, 125.9, 124.1, 122.9, 121.2, 116.9, 111.8. FTIR (KBr, wavenumber, cm^{-1}): 3058, 3029, 2213, 1644, 1587, 1485, 1425, 1331, 1282, 1201, 1177, 1075, 1027, 897, 836, 750, 693, 616, 539. MALDI-TOF (m/z): 666.37 [M^{+}]; calcd. for C$_{48}$H$_{34}$N$_4$: 666.28.
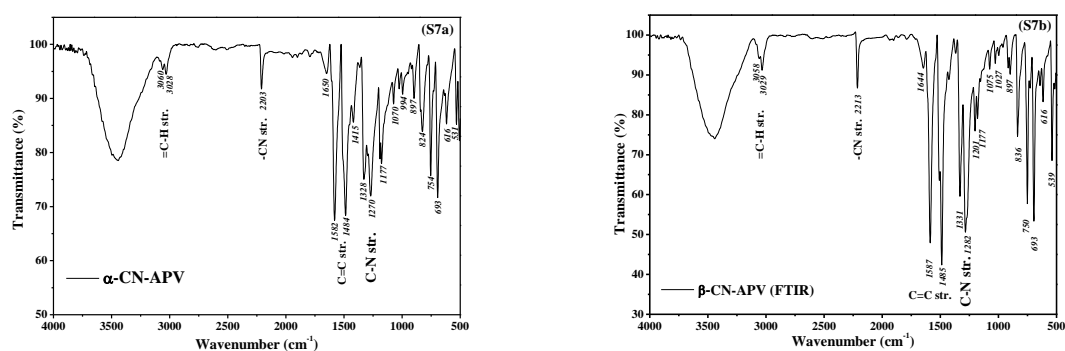
Figure S4. ^{1}H NMR (600 MHz, DMSO-d_6) of β-CN-APV

Figure S5. ^{13}C NMR (150 MHz, CDCl$_3$) of β-CN-APV.

Figure S6. Mass Spectrum (MALDI-TOF) of β-CN-APV.

Figure S7. FTIR (KBr, cm^{-1}) of α-CN-APV (S7a) and β-CN-APV (S7b).

Table S1 FTIR selected peaks assignment for the α-CN-APV and β-CN-APV

Functional Group	[a]α-CN-APV (cm^{-1})	[b]β-CN-APV (cm^{-1})
=C-H (str.) [c]	3060, 3028	3058, 3029
-CN str.	2203	2213
C=C str. [c]	1582, 1484, 1415	1587, 1485, 1425
C-N str. [c]	1270	1282
C-H oop [c]	826, 754, 693	836, 750, 693

[a,b]Data from Fig. S7a, S7b respectively; [c] Peak assignmentsare based on previous research (*J. Raman Spectrosc.* **2011**, *42*, 1682-1689).
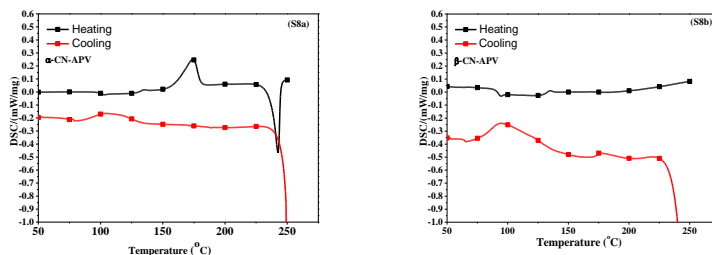
3. Thermal properties

Figure S8. DSC Curves of α-CN-APV (S8a) and β-CN-APV (S8b), at heating and cooling rates of 10 °C min^{-1} under nitrogen flushing.

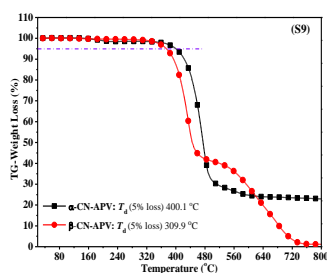**Figure S9.** TGA curves of α-CN-APV and β-CN-APV.

Table S2. Summary of the thermal properties

Thermal Parameter (°C)	α-CN-APV	β-CN-APV
$^{a}T_{g}$	103.3	94.2
$^{b}T_{m}$	174.2	131.2
$^{c}T_{c}$	103.2	93.2
$^{d}T_{d\,(5\%)}$	400	374.1

[a] T_g = glass transition temperature. [b] T_m = melting temperature.

[c] T_c = crystallization temperature. [d] $T_{d\,(5\%)}$ = Temperature at wt5% loss.

The thermal behaviours of the α-CN-APV and β-CN-APV were investigated by means of Differential Scanning Calorimetric (DSC, Fig.S8) and the thermogravimetric (TG) analyses (25-800 °C, Fig.S9) at standard heating and cooling rates of 10 °C/min under nitrogen flushing. The thermal data is summarised in TableS2. In the scans shown in Fig.S8a

and Fig.S8b, the samples were heated to 260 ℃ for α-CN-APV and β-CN-APV. Both the α-CN-APV and β-CN-APV show the glass transition temperature (T_g) in the heating cycle at 103.3 ℃ and 94.2 ℃. The α-CN-APV and β-CN-APV show the melting temperature (T_m) at 174.2 ℃ and 131.2 ℃. In the cooling cycle, α-CN-APV and β-CN-APV shows a crystallization peak (T_c) in the cooling cycle at 103.2 ℃ and 93.2 ℃. The T_d for 5% mass loss observed at 400 ℃ and 374 ℃ for the α-CN-APV and β-CN-APV respectively.

4. Electrochemical properties
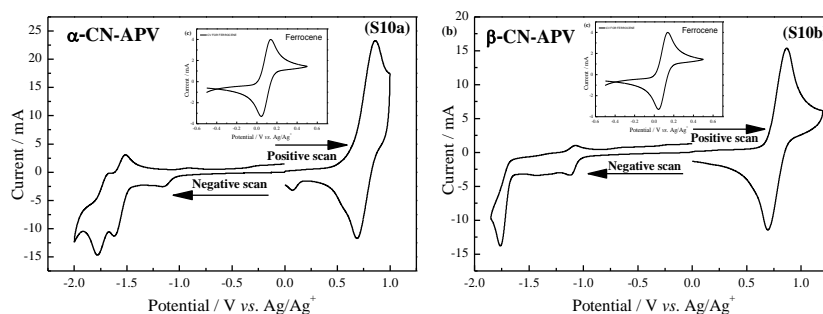

Figure S10. Cyclic Voltammograms (CV) of α-CN-APV and β-CN-APV. Working electrode: glassy-carbon disk; counter electrode: Pt wire; reference electrode: Ag/Ag$^+$. Scan rate: 50 mV s^{-1}. Electrolyte: 0.1 mol. L^{-1}, TBAPF$_6$ in MeCN.

Table S3. Electrochemical results from cyclic voltammetry of α-CN-APV and β-CN-APV.

Oligomer	[a]E_{ox} (V) /[d]HOMO (eV)	[b]E_{red} (V) /[e]LUMO (eV)	[c]E_g^{ec} (eV)
α-CN-APV	0.64/-5.35	-1.49/-3.22	2.13
β-CN-APV	0.69/-5.4	-1.67/-3.04	2.36

[a] Oxidation onset potential. [b] Reduction onset potential.

[c] Electrochemical Band gap. [d] Energy of HOMO level.

[e] Energy of LUMO level.

The cyclic voltammograms (CVs) of α-CN-APV and β-CN-APV in CH$_3$CN solutions are shown in Fig. S10 and the comparison of the electrochemical properties are summarized in the Table S3. Both the CVs show oxidation peak with the onset oxidation (positive scan) potentials at 0.64 and 0.69 V (vs. Ag/Ag$^+$), respectively. The α-CN-APV and β-CN-APV show the onset-reduction potentials (negative-scan) at -1.49 eV and -1.67 eV. The E_{HOMO} and E_{LUMO} levels were estimated from the onset-oxidation and reduction potentials respectively by comparison to that of ferrocene according to the following equations: $E_{\text{HOMO}} = - (E_{ox}$ vs. Ag/Ag$^+$ - $E_{1/2}$ vs. Ag/Ag$^+$ + 4.8) eV; E_{LUMO} = - (E_{red} vs. Ag/Ag$^+$ - $E_{1/2}$ vs. Ag/Ag$^+$ + 4.8) eV. Where the E_{ox} vs. Ag/Ag$^+$ and E_{red} vs. Ag/Ag$^+$ are the oxidation and reduction onset potentials relative to the Ag/Ag$^+$ electrode, respectively. The $E_{1/2}$ vs. Ag/Ag$^+$ is the half wave potentials ($E_{1/2} = (E_{pa} + E_{pc})/2$; 0.09 V) of Fc/Fc$^+$. The calculation gives

HOMO energy level, E_{HOMO} for the α-CN-APV = -5.3 eV and -5.4 eV for the β-CN-APV. Similarly the E_{LUMO} levels calculated from the onset-reduction potentials are: E_{LUMO} for the α-CN-APV = -3.22 eV and -3.04 eV for the β-CN-APV. The electrochemical band gaps (E_g^e) for the α-CN-APV and β-CN-APV are 2.13 eV and 2.36 eV respectively.
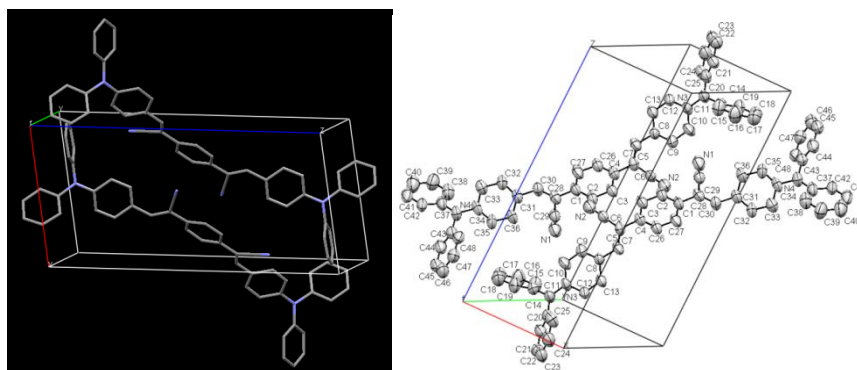
5. **X-ray Crystallography**

Figure S11. Unit cell for the *α*-CN-APV (Carbon: Grey; Nitrogen: Sky blue; red line: *a*-axis, green line: *b*-axis, blue line: *c*-axis).

Table S4 Crystal Data and Structure Refinement for ***α*-CN-APV.**

CODE NAME	*α*-CN-APV
Empirical formula	$C_{48}H_{34}N_4$
Formula weight	666.79
Temperature (K)	293 (2)
Wavelength (Å)	0.71073
Crystal system	Triclinic
Space group	P-1
Unit cell dimensions	
a (Å)	9.5046(19)
b (Å)	9.874(2)
c (Å)	19.372(4)
α (°)	81.04(3)
β (°)	81.10(3)
γ (°)	89.66(3)
Volume (Å³)	1773.9(6)
Z, density_diffrn (mg/m³), R(%)	2, 1.248, 11.6
Absorption Coefficient (mm⁻¹)	0.073
F (000)	700
Theta ranges for data collection (°)	2.99-27.48
Limiting indices	-12<=h<=12, -12<=k<=12,

	$-23 <= l <= 25$
Reflections collected/unique	8059/1885 [R_{int} = 0.2121]
Refinement method	Full-matrix least-squares on F^2
Final R indices [I > 2σ(I)]	R_1 = 0.0531, wR_2 = 0.3062
R indices (all data)	R_1 =0.1160, wR_2 = 0.4388
Goodness-of-fit on F^2	0.968

The intensity data for the singlecrystal X-ray diffractionanalysis of two Molecules were collected at room temperature on diffractometer using MoKαradiation (λ=0.71073 Å). Data collection was performed with COLLECT cell refinementand data reduction with DENZO/SCALEPACK. The structure was solved with SHELXL-97 was used for full matrix least squares refinement. The H-atoms werethen introduced at idealized positions and constraint to their parent atom during thelast refinements. Graphics were generated with MERCURY 2.4.The crystallographic data for the structure determination and refinement of the two compounds are presented in the attached cif files, Table S4 and Table S5. CCDC 1450594 and CCDC 1450595 contain the supplementary crystallographic data for the two compounds. The data can be obtained free of charge via http://www.ccdc.cam.ac.uk.
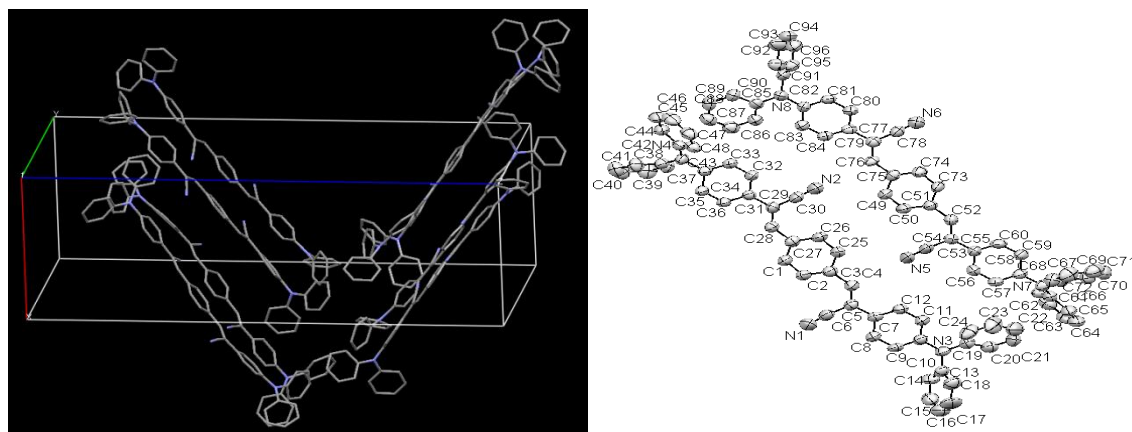

Figure S12. Unit cell for the *β*-CN-APV (Carbon: Grey; Nitrogen: Sky blue; red line: *a*-axis, green line: *b*-axis, blue line: *c*-axis).

Table S5. Crystal Data and Structure Refinement for β-CN-APV.

CODE NAME	β-CN-APV
Empirical formula	$C_{48}H_{34}N_4$
Formula weight	666.79
Temperature (K)	293(2)
Wavelength (Å)	0.71073
Crystal system	*Orthorhombic*
Space group	$Pca2_1$
Unit cell dimensions	
a (Å)	12.279(3)
b (Å)	16.264(3)
c (Å)	36.106(7)
α (^{o})	90.00
β (^{o})	90.00
γ (^{o})	90.00
Volume (Å^3)	7211(3)
Z, density-diffrn (mg/m^3), R(%)	8, 1.228, 5.31
Absorption Coefficient (mm^{-1})	0.072
F (000)	2800
Theta ranges for data collection (^{o})	3.00 - 27.47
Limiting indices	$-15<=h<=15$, $-20<=k<=21$, $-41<=l<=46$
Reflections collected/ unique	15305/4251[R_{int} = 0.2121]
Refinement method	Full-matrix least-squares on F^2
Final R indices [I > 2σ(I)]	$R_1 = 0.0531, wR_2 = 0.0843$
R indices (all data)	$R_1 = 0.2423, wR_2 = 0.1358$
Goodness-of-fit on F^2	0.823

Table S6. Selected Torsion Angles in the Crystal Structures of the *α*-CN-APV and *β*-CN-APV (from cif files).

Material	Torsion Angles (deg.)					
α-CN-APV	C3-C4-C5-C6	C6-C5-C7-C8	C5-C7-C8-C9	C2-C1-C28-C29	C29-C28-C30-C31	C28-C30-C31-C36
	-14.7	-11	-24	2	4	23
β-CN-APV	C2-C3-C4-C5	C6-C5-C7-C8	C4-C5-C7-C12	C26-C27-C28-C29	C27-C28-C29-C30	C30-C29-C31-C32
	5	-12.3	-11.7	4	4	-14.1

6. Photograph of *α*-CN-APV and *β*-CN-APV
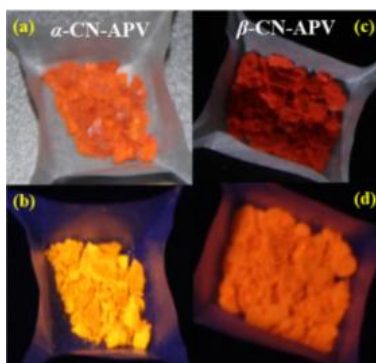
Figure S13. Fluorescence photograph of *α*-CN-APV and *β*-CN-APV under day-light (a, c) and UV-lamp (b, d).
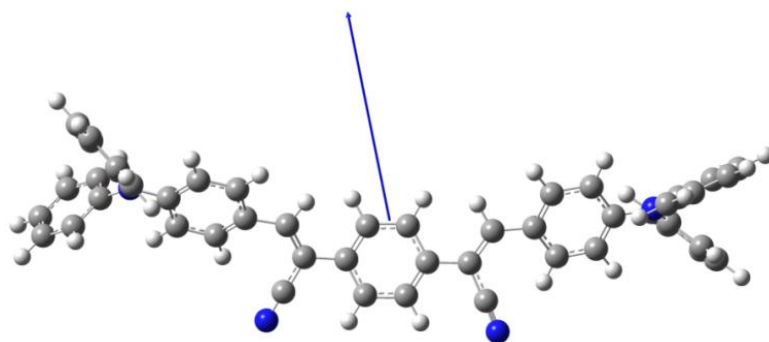
7. Ground-state dipole moments and molecular configurations

Figure S14. Ground-state dipole moment (blue vector near central benzene) calculated from the crystal structure of the *α*-CN-APV.
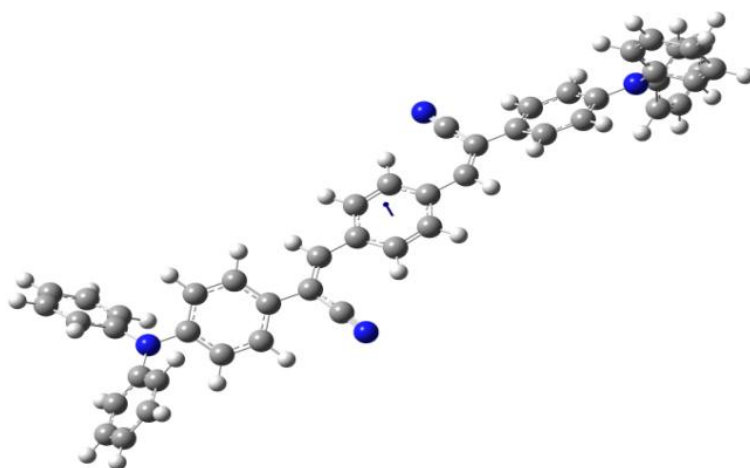

Figure S15. Ground-state dipole moment (blue vector inside, perpendicular to central benzene) calculated from the crystal structure of the *β*-CN-APV.
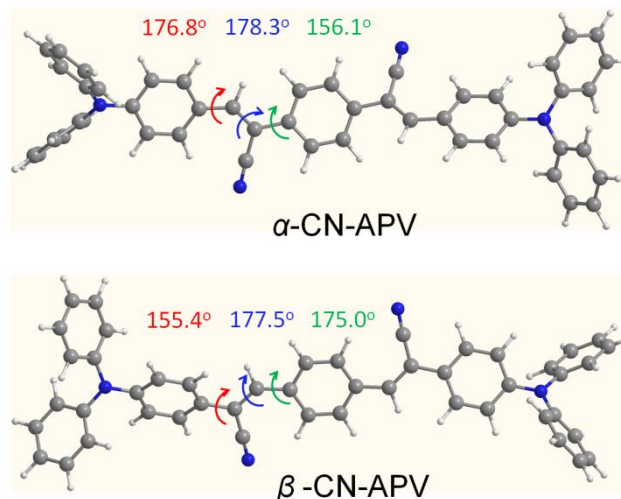
Figure S16. The optimized molecular structures of α-CN-APV and β-CN-APV.

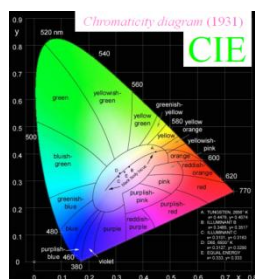## 8. EL Color Characterization

Figure S17 Commission Internationale de L'Eclairage (CIE) diagram for accurate color

measurements.

The OLED made from *α*-CN-APV showed EL emission peak at 530 nm with CIE (0.365, 0.602). These coordinates on CIE (Fig.S16) show a green emission close to the top of CIE triangle. The OLED made from *β*-CN-APV showed EL emission peak at 566 nm with CIE (0.495, 0.499). These coordinates on CIE diagram show a yellow emission between the top green and right red-corner.

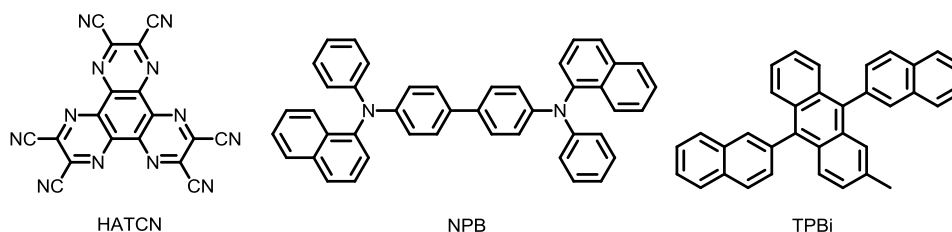## 9. Chemical Structures of the Materials Used in EL Devices

Chart S1. Chemical structures of HATCN, NPB, MADN and TPBi.